JCTC Journal of Chemical Theory and Computation

Gaussian Basis Set and Planewave Relativistic Spin−Orbit Methods in NWChem

Patrick Nichols,* Niranjan Govind,* Eric J. Bylaska, and W. A. de Jong

William R. Wiley Environmental Molecular Sciences Laboratory, Pacific Northwest National Laboratory, 902 Battelle Boulevard, P.O. Box 999, Mail Stop K8-91, Richland, Washington, 99352

Received July 21, 2008

Abstract: Relativistic spin−orbit density functional theory (DFT) methods have been implemented in the molecular Gaussian DFT and pseudopotential planewave DFT modules of the NWChem electronic-structure program. The Gaussian basis set implementation is based upon the zeroth-order regular approximation (ZORA) while the planewave implementation uses spin−orbit pseudopotentials that are directly generated from the atomic Dirac−Kohn−Sham wave functions or atomic ZORA-Kohn−Sham wave functions. Compared to solving the full Dirac equation these methods are computationally efficient but robust enough for a realistic description of relativistic effects such as spin−orbit splitting, molecular orbital hybridization, and core effects. Both methods have been applied to a variety of small molecules, including I_2, IF, HI, Br_2, Bi_2, AuH, and Au_2, using various exchange-correlation functionals. Our results are in good agreement with experiment and previously reported calculations.

I. Introduction

It is well established that scalar and spin−orbit relativistic effects have to be taken into account for accurate electronic structure calculations of actinides and other heavy elements. Relativistic effects are best described in electronic-structure calculations by solving the Dirac equation, whose solutions are made up of four-component spinor wave functions. However, four-component methods are not only fraught with problems such as variational collapse,[1] they are also an order of magnitude more expensive. The extra cost stems from the need to properly describe the small component wave function. In principle, the cost of the Dirac equation can be reduced by transforming it from a regular four-component eigenvalue equation into a nonregular two-component eigenvalue equation by decoupling the large and small components of the wave function. However, this nonregular two-component eigenvalue equation turns out to be difficult to solve, because it has a nontrivial normalization condition and the eigenvalue depends nonlinearly upon itself. Over the years, many approximations have been developed to circumvent these difficulties such as the Breit−Pauli Hamiltonian, direct perturbation theory, Dyall's modified Dirac method,[2] and the Douglas−Kroll−Hess (DKH) Hamiltonian.[3−5] Another approximation, the zeroth-order regular approximation (ZORA) method, has become one of the more popular of these approximations. The ZORA method was originally developed by Chang and Durand.[6] This method was rediscovered and further developed by Baerends, van Lenthe, and co-workers.[7] It is a two-component spinor approach for approximately solving the Dirac equation based upon regularizing the wave equation by ignoring the energy dependence of the effective mass of the electron. It has been shown that the solutions of the ZORA equation are one of the best two-component approximations to the fully relativistic Dirac solution for hydrogen-like systems. Since this is a two-component method, calculations can be performed using only the large component. This approximation has been shown to perform well for a wide variety of properties and is among the cheapest of the approximate spinor methods.[8,9]

The ZORA approximation and other regularized two-component methods can be used to solve for all the electrons (core + valence) in the system. However, this is not typically necessary, since the most significant relativistic effects are in the core region and can be encapsulated using core potentials (RECP)[10−12] or pseudopotentials.[13−15] These types

* Corresponding authors. E-mail: patrick.nichols@pnl.gov (P.N.), niri.govind@pnl.gov.

10.1021/ct8002892 CCC: $40.75
Published on Web 01/28/2009

of approaches have been shown to give accurate structures, frequencies, and other properties that depend primarily on getting the valence electronic structure correct. For properties that directly involve core orbitals such as XPS and NMR, all-electron methods may be needed. Relativistic pseudopotentials with spin−orbit effects have been also been developed in the past. The HGH pseudopotentials are among the most well-known.[13] The Helmstreet, Fong, and Nelson pseudopotential is another example.[16] Theurich and Hill have also developed a pseudopotential for III−V semiconductors that is similar to the one implemented here for the norm-conserving case.[17,18] Ultrasoft pseudopotentials incorporating spin−orbit effects have also been studied, e.g. Corso and co-workers[14,15] and the work of Oda and Hosokawa.[19] Chelikowsky and co-workers have recently extended these approaches to real space grids.[20] Solid-state calculations using these approaches have all yielded favorable results for both geometries and spin−orbit splittings.

In this paper we present our implementation and applications of the relativistic two-component Hamiltonian within the Gaussian basis set and planewave frameworks. Both spin-free and spin−orbit versions of the Hamiltonian have been implemented. In the formalism and implementation section, we present a short overview of the theory and the details of our implementation in the framework of the NWChem program package.[21] To test our implementation, we have calculated the equilibrium geometries, harmonic frequencies, and dissociation energies for a set of small closed-shell molecules (I_2, Br_2, HI, IF, Au_2, Bi_2, AuH). We compare the results using various exchange-correlation functionals within the spin-free and spin−orbit approaches. The results are also compared with experimental data and published calculations.

II. Formalism and Implementation

A. ZORA Formalism. The two-component ZORA equation is given by

$$\left[\boldsymbol{\sigma}\cdot\mathbf{p}\frac{K(\mathbf{r})}{2m_e}\boldsymbol{\sigma}\cdot\mathbf{p}+V(\mathbf{r})\right]\psi_n(\mathbf{r})=\epsilon_n^{\mathrm{ZORA}}\psi_n(\mathbf{r}) \quad (1)$$

where

$$K(\mathbf{r})=\left(1-\frac{V(\mathbf{r})}{2m_ec^2}\right)^{-1} \quad (2)$$

After some algebra, eq 1 can be written as

$$\left[\mathbf{p}\frac{K(\mathbf{r})}{2m_e}\mathbf{p}+\frac{(K(\mathbf{r}))^2}{4m_e^2c^2}\boldsymbol{\sigma}\cdot(\nabla V(\mathbf{r})\times\mathbf{p})+V(\mathbf{r})\right]\psi_n(\mathbf{r})=\epsilon_n^{\mathrm{ZORA}}\psi_n(\mathbf{r}) \quad (3)$$

As one can see above, the spin−orbit operator (term 2) in eq 3 is already present at this lowest-order of the expansion. Equation 1 can also be written as

$$\left[\frac{\mathbf{p}^2}{2m_e}+\mathbf{p}\left(\frac{K(\mathbf{r})-1}{2m_e}\right)\mathbf{p}+\frac{(K(\mathbf{r}))^2}{4m_e^2c^2}\boldsymbol{\sigma}\cdot(\nabla V(\mathbf{r})\times\mathbf{p})+V(\mathbf{r})\right]\psi_n(\mathbf{r})=\epsilon_n^{\mathrm{ZORA}}\psi_n(\mathbf{r}) \quad (4)$$

where the nonrelativistic kinetic energy contribution has been isolated. The advantage of this decomposition is that the ZORA contribution can be treated as a correction which can be added to the kinetic-energy matrix elements and also recovers the correct limits in addition. The spin-free or scalar-relativistic equation can be obtained by eliminating the spin−orbit term, resulting in the following equation,

$$\left[\frac{\mathbf{p}^2}{2m_e}+\mathbf{p}\left(\frac{K(\mathbf{r})-1}{2m_e}\right)\mathbf{p}+V(\mathbf{r})\right]\psi_n(\mathbf{r})=\epsilon_n^{\mathrm{ZORA}}\psi_n(\mathbf{r}) \quad (5)$$

It has been established that the one-electron energies of the ZORA equation, $\epsilon_i^{\mathrm{ZORA}}$, can be improved by scaling the ZORA energy.[8,9] This scaling essentially captures the effects of summing certain higher-order contributions to infinite order. The scaled one-electron energies $\epsilon_i^{\mathrm{scaled}}$ are given by

$$\epsilon_i^{\mathrm{scaled}}=\frac{\epsilon_i^{\mathrm{ZORA}}}{1+\langle\phi_i(\mathbf{r})|\boldsymbol{\sigma}\cdot\mathbf{p}\frac{(K(\mathbf{r}))^2}{4m_e^2c^2}\boldsymbol{\sigma}\cdot\mathbf{p}|\phi_i(\mathbf{r})\rangle} \quad (6)$$

Within the density functional theory (DFT) framework, the total scaled ZORA energy E_{tot}^{s} can be written as

$$E_{\mathrm{tot}}^{\mathrm{scaled}}=\sum_{i=1}^{N}\left[\langle\phi_i(\mathbf{r})|\boldsymbol{\sigma}\cdot\mathbf{p}\frac{K(\mathbf{r})}{2m_e}\boldsymbol{\sigma}\cdot\mathbf{p}|\phi_i(\mathbf{r})\rangle-\epsilon_i^{\mathrm{scaled}}\langle\phi_i(\mathbf{r})|\boldsymbol{\sigma}\cdot\mathbf{p}\frac{(K(\mathbf{r}))^2}{4m_e^2c^2}\boldsymbol{\sigma}\cdot\mathbf{p}|\phi_i(\mathbf{r})\rangle\right]+\int \mathrm{d}r\,\rho(\mathbf{r})V_{\mathrm{ion}}(\mathbf{r})+\frac{1}{2}\iint \mathrm{d}\mathbf{r}\,\mathrm{d}\mathbf{r}'\,\frac{\rho(\mathbf{r})\rho(\mathbf{r}')}{|\mathbf{r}-\mathbf{r}'|}+E_{\mathrm{xc}}[\rho(\mathbf{r})]+E_{nn} \quad (7)$$

where the summation runs over the occupied orbitals. The above equation is identical to the nonrelativistic total energy except for the kinetic energy contribution which includes the ZORA correction.

B. Gaussian Basis Implementation. In our Gaussian basis set implementation, the molecular spinors are expanded in terms of real basis functions as follows,

$$\phi_i(\mathbf{r})=\sum_\mu\left\{c_{\mu i}^{\alpha}\begin{pmatrix}\chi_\mu(\mathbf{r})\\0\end{pmatrix}+c_{\mu i}^{\beta}\begin{pmatrix}0\\\chi_\mu(\mathbf{r})\end{pmatrix}\right\}=\begin{pmatrix}\phi_i^{\alpha}(\mathbf{r})\\\phi_i^{\beta}(\mathbf{r})\end{pmatrix} \quad (8)$$

where χ_μ are Gaussian basis functions and $c_{\mu i}^{\alpha}$ and $c_{\mu i}^{\beta}$ are expansion coefficients which are, in general, complex. Since the ZORA corrections only affect the kinetic energy, we only concentrate on this term. The remaining terms are evaluated in the conventional manner within the molecular Gaussian DFT module in NWChem. Within the basis set approximation and using the decomposition from eq 4, the corrected kinetic energy elements of the Fock matrix can be written as

$$T_{\mu\nu}^{\mathrm{tot}}=\langle\chi_\mu(\mathbf{r})|\frac{\mathbf{p}^2}{2m_e}|\chi_\nu(\mathbf{r})\rangle+\langle\chi_\mu(\mathbf{r})\boldsymbol{\sigma}\cdot\mathbf{p}|\frac{K(\mathbf{r})-1}{2m_e}|\boldsymbol{\sigma}\cdot\mathbf{p}\chi_\nu(\mathbf{r})\rangle \quad (9)$$

The spin-free or scalar-relativistic case can be obtained in a similar way using eq 5. In NWChem, the nonrelativistic part of the kinetic energy (first term in the above equation) is evaluated analytically where as the ZORA correction (second term) is calculated numerically on atom-centered grids.[25] Since the ZORA correction depends on the potential, it is not gauge invariant. There have been a number of attempts

to address this issue.[22−24] In our implementation, we address this by using the atomic approximation of van Lenthe and co-workers.[26,27] Strictly speaking none of these methods are truly gauge invariant in the general sense, but they help minimize the problem. Within the atomic approximation, the ZORA corrections to the kinetic energy matrix elements are calculated using the superposition of densities of the atoms in the system. As a result, only intra-atomic contributions are involved and no gradient or second derivatives of these corrections need to be calculated. In addition, the corrections only have to be calculated once and stored. With this, we can re-express eq 9 as

$$T_{\mu\nu}^{\mathrm{tot}} = \langle \chi_\mu(\mathbf{r}) | \frac{\mathbf{p}^2}{2m_e} | \chi_\nu(\mathbf{r}) \rangle + \langle \chi_\mu(\mathbf{r}) \boldsymbol{\sigma}\cdot\mathbf{p} | \frac{\tilde{K}(\mathbf{r})-1}{2m_e} | \boldsymbol{\sigma}\cdot\mathbf{p}\chi_\nu(\mathbf{r}) \rangle \tag{10}$$

where $\tilde{K}(\mathbf{r}) = (1 - \tilde{V}(\mathbf{r})/2m_e c^2)^{-1}$ and $\tilde{V} \approx V_{\mathrm{atom}}^{\mathrm{ne}} + V_{\mathrm{atom}}^{\mathrm{H}}$, the sum of the atomic nuclear-electron, Hartree potentials, respectively. The atomic densities are calculated for the neutral atoms at the Hartree−Fock (HF) level, and then, the ZORA potential corrections are calculated using this density. Note that we ignore the exchange-correlation contribution in the evaluation of the ZORA atomic corrections in the same way as van Lenthe and co-workers.[26,27,33] This approximation works well, as shown by our results. Our implementation differs from theirs in that they use a resolution of identity (RI) approach to calculate the ZORA corrections while we use atom-centered grids.

C. Planewave Implementation. The planewave implementation uses a two-component spinor expanded in planewaves as a basis to describe the eigenfunctions of the system.

$$\psi_i(\mathbf{r}) = \begin{bmatrix} \psi_i^\alpha(\mathbf{r}) \\ \psi_i^\beta(\mathbf{r}) \end{bmatrix} \tag{11}$$

where

$$\int \mathrm{d}^3 r \, (\psi_i^{\alpha *}(\mathbf{r})\psi_i^\alpha(\mathbf{r}) + \psi_i^{\beta *}(\mathbf{r})\psi_i^\beta(\mathbf{r})) = 1 \tag{12}$$

The Hamiltonian operator acts upon the two-component spinor planewaves in the usual fashion. For a single eigenfunction,

$$\begin{bmatrix} H_{\alpha\alpha} & H_{\alpha\beta} \\ H_{\beta\alpha} & H_{\beta\beta} \end{bmatrix} \begin{bmatrix} \psi_i^\alpha(\mathbf{r}) \\ \psi_i^\beta(\mathbf{r}) \end{bmatrix} = \begin{bmatrix} \epsilon\psi_i^\alpha(\mathbf{r}) \\ \epsilon\psi_i^\beta(\mathbf{r}) \end{bmatrix} \tag{13}$$

and the generalization to many eigenfunctions is of similar form. Relativistic effects are most dominant in the deep core region. Since we are mainly interested in the valence properties, one can encapsulate the core effects into a pseudopotential. In this work, we construct a two-component nonlocal pseudopotential. This potential will in general act on the spin up and spin down components of each eigenfunction in a nontrivial fashion. The first step in generating a relativistic pseudopotential is to solve for the two-component spinor all-electron wave functions and the self-consistent potential for the atom using either two-component radial Dirac or ZORA equation. The large two-component solutions are of the form

$$\psi_{njlm_j}(\mathbf{r}) = \frac{u_{njl}(r)}{r} \mathscr{Y}_l^{j,m_j}(\hat{r}) \tag{14}$$

where $u_{jl}(r)$ is the radial wave function, $\mathscr{Y}_l^{j,m_j}$ is a spin angular function, and the principal quantum numbers are n, j, l, and j_3 where $n \in [1, 2, 3,...]$, $l \in [0, 1, 2,..., n-1]$, $j = l \pm {}^1/_2$ and $m_j \in [-j, -j+1,..., 0,..., (j-1), j]$. The spin angular functions, which are eigenfunctions of J^2, J_z, and $\boldsymbol{\sigma}\cdot\mathbf{L}$, are defined to be for $j = l + {}^1/_2$

$$\mathscr{Y}_l^{j,m_j}(\hat{\mathbf{r}}) = \begin{bmatrix} \sqrt{\dfrac{j+m_j+\frac{1}{2}}{2l+1}} Y_l^{m_j-1/2}(\hat{\mathbf{r}}) \\ \sqrt{\dfrac{j-m_j+\frac{1}{2}}{2l+1}} Y_l^{m_j+1/2}(\hat{\mathbf{r}}) \end{bmatrix} \tag{15}$$

and for $j = l - {}^1/_2$

$$\mathscr{Y}_l^{j,m_j}(\hat{\mathbf{r}}) = \begin{bmatrix} -\sqrt{\dfrac{j-m_j+\frac{1}{2}}{2l+1}} Y_l^{m_j-1/2}(\hat{\mathbf{r}}) \\ \sqrt{\dfrac{j+m_j+\frac{1}{2}}{2l+1}} Y_l^{m_j+1/2}(\hat{\mathbf{r}}) \end{bmatrix} \tag{16}$$

where Y_l^m are the spherical harmonic functions.[28] We can convert the all-electron radial valence wave functions $u_{njl}(r)$ to radial pseudowave functions, $w_{jl}(r)$, and corresponding screened ionic pseudopotentials, $V_{jl}^{\mathrm{scr,ion}}$ by inverting the radial Schrödinger equation using the Hamann[29] or Troullier−Martins procedure.[30] The screened ionic pseudopotential components are then unscreened (ignoring the small component contribution to the valence density for Dirac solutions and the corresponding change in wave function normalization)

$$V_{jl}^{\mathrm{ion}}(r) = V_{jl}^{\mathrm{scr,ion}}(r) - V_{\mathrm{xc}}[\rho_{\mathrm{val}}(r)] - V_{\mathrm{H}}[\rho_{\mathrm{val}}(r)] \tag{17}$$

where $V_{\mathrm{xc}}[\rho_{\mathrm{val}}(r)]$ and $V_{\mathrm{H}}[\rho_{\mathrm{val}}(r)]$ are the exchange-correlation and Hartree functional potentials due to the pseudovalence density, $\rho_{\mathrm{val}}(r)$.

The two-component semilocal pseudopotential operators are of the following form,

$$\hat{V}^{\mathrm{ps}} = \sum_{j,l,m_j} |_c\mathscr{Y}_l^{j,m_j}\rangle \, V_{jl}^{\mathrm{ion}}(r) \langle_c\mathscr{Y}_l^{j,m_j}| \tag{18}$$

One can decompose V_{jl}^{ion} as follows

$$V_{jl}^{\mathrm{ion}}(r) = \bar{V}_l(r) + \langle \sigma\cdot\mathbf{L} \rangle_{jl} V_l^{\mathrm{so}}(r) \tag{19}$$

where $\bar{V}_l$ denotes the l-averaged scalar relativistic pseudopotential, V_l^{so} denotes the radial spin−orbit pseudopotential component, and

$$\langle \sigma\cdot\mathbf{L} \rangle_{jl} = \begin{cases} \dfrac{l}{2} & \text{for } j = l + \dfrac{1}{2} \\ -\dfrac{l+1}{2} & \text{for } j = l - \dfrac{1}{2} \end{cases} \tag{20}$$

are the expectation values of the spin−orbit operator. Given that

$$V_{j=l+1/2,l}^{\mathrm{ion}}(r) = \bar{V}_l(r) + \frac{l}{2} V_l^{\mathrm{so}}(r) \tag{21}$$

$$V^{\text{ion}}_{j=l-1/2,l}(r) = \bar{V}_l(r) - \frac{1}{2}(l+1)V^{\text{so}}_l(r) \tag{22}$$

one can readily solve for the *l*-averaged and spin−orbit potentials.

$$\bar{V}_l = \frac{(l+1)V^{\text{ion}}_{j=l+1/2,l} + lV^{\text{ion}}_{j=l-1/2,l}}{2l+1} \tag{23}$$

$$V^{\text{so}}_l(r) = \frac{2}{2l+1}(V^{\text{ion}}_{j=l+1/2,l} - V^{\text{ion}}_{j=l-1/2,l}) \tag{24}$$

The radial ionic pseudopotentials and radial pseudowave functions are shown in Figures 1 and 2, respectively, for the case of bismuth. For the s and d states, all three methods are in complete agreement. For the p states, the ZORA and Dirac results agree almost exactly while the scalar Dirac clearly shows the effects of the averaging procedure. The results for *j*-averaged pseudopotential, $\bar{V}_l$, are shown in Figure 3. Note that all three methods produce identical functions for this atom. In Figure 4, one sees that for the spin−orbit term, V^{so}_l, Dirac and ZORA once again provide identical results. Analogous to the form given by Hamann,[29] the full pseudopotential matrix element assumes the form,

$$\langle\phi_1|\hat{V}^{\text{ps}}|\phi_2\rangle = \sum_{j,l,m_j}\int d^3r \int d^3r'\, \phi^*_1(\mathbf{r})\mathscr{Y}^{j,m_j}_l(\hat{r})V^{\text{ion}}_{jl}(r)\delta(r-r')\mathscr{Y}^{j,m_j\ddagger}_l(\hat{r}')\phi_2(r') \tag{25}$$

where the ion is centered at the origin. The Kleinman−Bylander expansion of this expression[31] is given by

$$\langle\phi_1|\hat{V}^{\text{ps}}(\mathbf{r})|\phi_2\rangle = \langle\phi_1|V^{\text{local}}|\phi_2\rangle + \sum_{\kappa,J_3} C_\kappa\langle\phi_1|V^{\text{nonlocal}}_{jl}|\phi_2\rangle \tag{26}$$

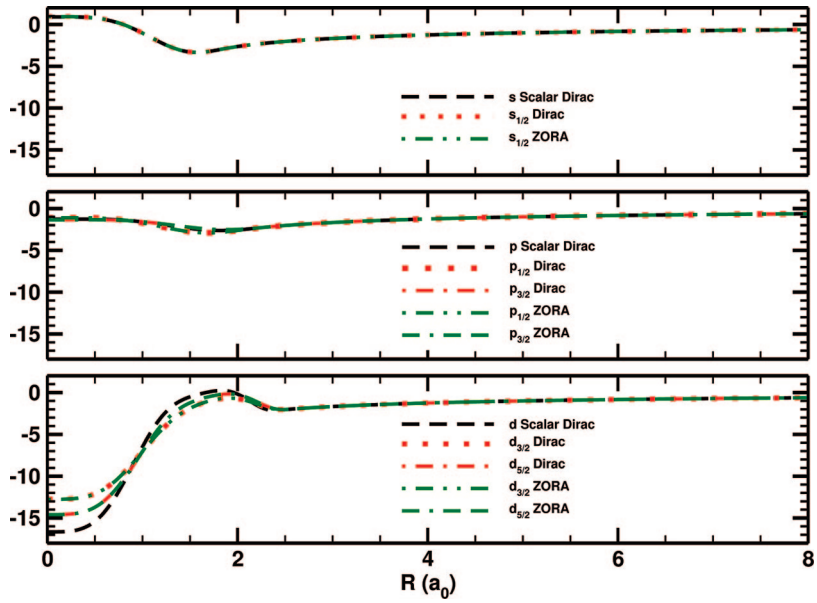

Figure 1. Ionic spin angular pseudopotentials (**L** = s, p, d) for Bismuth using Scalar Dirac, Dirac, and ZORA.

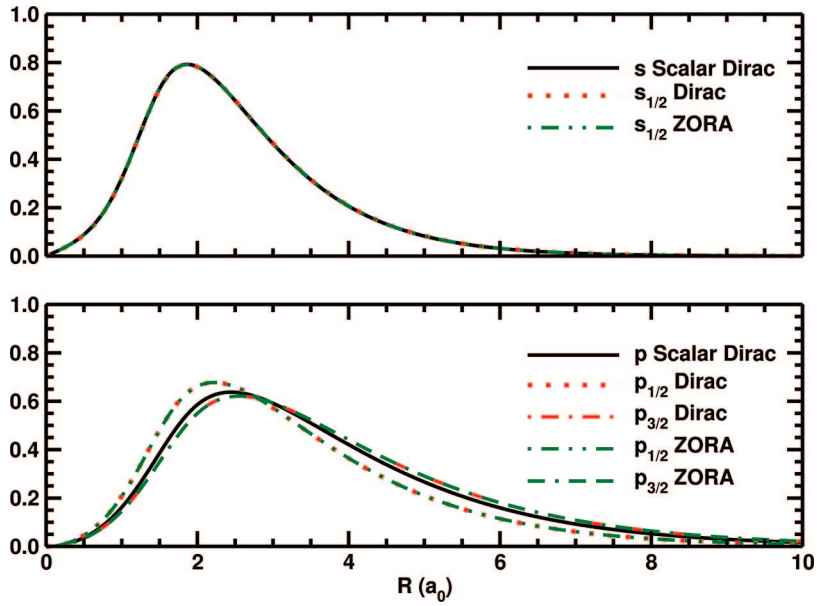

Figure 2. Radial component of the spin angular pseudowave functions (**L** = s, p) for bismuth using Scalar Dirac, Dirac, and ZORA.

where ϕ_1 and ϕ_2 are Pauli spinor planewave functions of the form

$$\phi_1(\mathbf{r}) = j_l(kr)\mathcal{Y}_l^{j,m_j}(\hat{\mathbf{r}}) \tag{27}$$

and the local potential matrix element is taken to be that of the nonrelativistic form, ($V^{\text{local}}(r) = \bar{V}_{l=l_{\text{local}}}(r)$),

$$\langle\phi_1|V^{\text{local}}|\phi_2\rangle = \int \mathrm{d}^3r\, \phi_1(\mathbf{r})\bar{V}_l(r)Y_l^m(\hat{r})\phi_2(\mathbf{r}) \tag{28}$$

and

$$\langle\phi_1|V_{jl}^{\text{nonlocal}}|\phi_2\rangle = \int \mathbf{d}^3r\, \phi_1^*(\mathbf{r})\mathcal{Y}_l^{j,m_j}(\hat{r})Q_{jl}^{\text{ion}}(r)\int \mathrm{d}^3r'\, \mathcal{Y}_l^{j,m_j\ddagger}(\hat{r}')Q_{jl}^{\text{ion}*}(r')\phi_2(\mathbf{r}') \tag{29}$$

The scalar radial term, $Q_{jl}^{\text{ion}}(r)$, is defined as

$$Q_{jl}^{\text{ion}}(r) = v_{jl}(r)\frac{w_{jl}(r)}{r} \tag{30}$$

the term C_{jl} is

$$C_{jl} = [4\pi\int_0^\infty r\,\mathrm{d}r\, Q_{jl}^{\text{ion}}w_{jl}(r)]^{-1} \tag{31}$$

and the nonlocal pseudopotential term, $v_{jl}(r) = V_{jl}^{\text{ion}}(r) - V^{\text{local}}(r)$. It should be pointed out that, in this prescription, neither of the two nonlocal potentials corresponding to the orbital angular momentum eigenstate l_{local} vanish, which is the case for the nonrelativistic prescription of standard pseudopotentials. In fact, each has parts of the spin−orbit interaction. Also, one must note that the local potential must be chosen carefully to ensure that C_{jl} does not diverge. For example, if integral containing v_{jl} that appears in the denominator is small this coefficient will be very large. Any error in the projector will be unreasonably amplified. The approach taken here is to set C_{jl} to zero when this occurs. Another noteworthy fact is that the nonlocal potential is an outer product of two spinor wave functions effectively making it a 2 × 2 complex matrix.

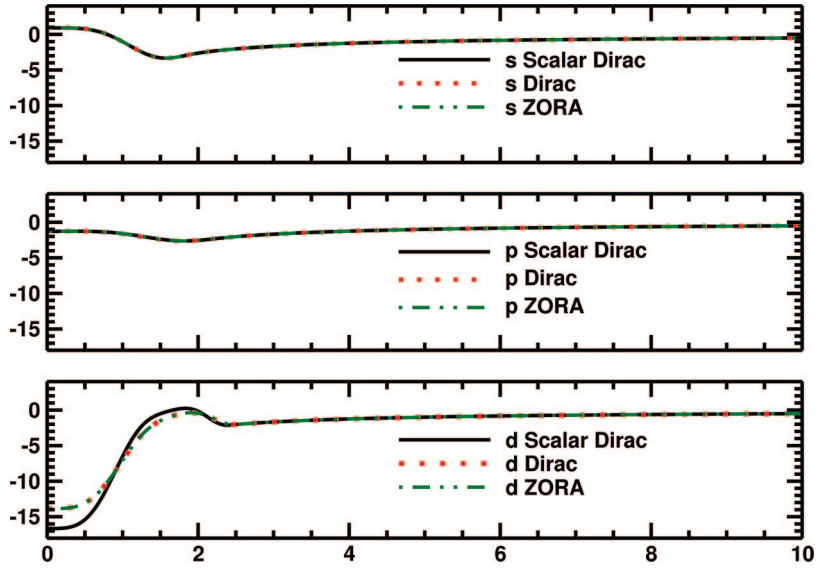

Figure 3. *l*-Averaged radial pseudopotentials (**L** = s, p, d) for bismuth using Scalar Dirac, Dirac, and ZORA.

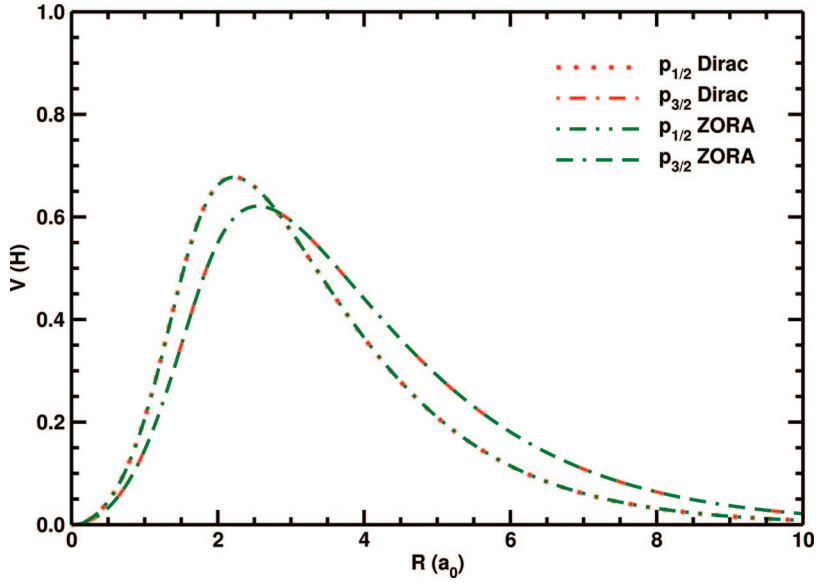

Figure 4. Radial spin−orbit component of pseudopotential (L = p) for bismuth using Scalar Dirac, Dirac, and ZORA.

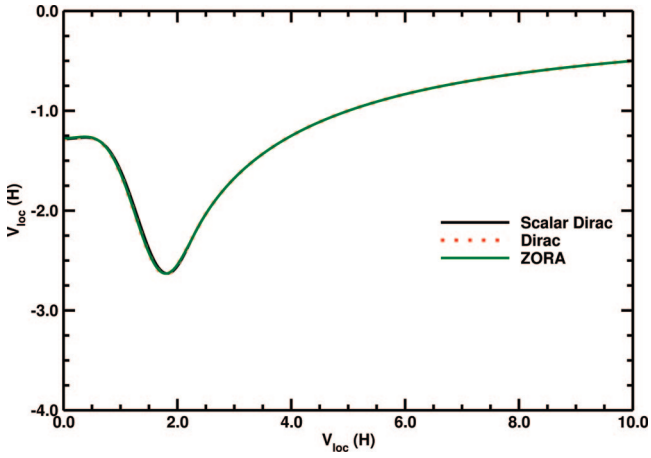

Figure 5. Radial local potential (**L** = p) for bismuth using Scalar Dirac, Dirac, and ZORA.

These quantities for the three methods are shown in Figure 6. As was the case, for the ionic pseudopotentials, the p and d states show very close to exact agreement between ZORA and Dirac, while the scalar Dirac method is clearly an averaged outcome for the two values of j for each l. The crucial feature of this new pseudopotential is that the projectors are two-component spinors. Thus, when the Kleinman−Bylander expansion is done, we are expanding in terms of the eigenvalues of the spin angular functions instead of scalar functions which are eigenfunctions of the angular momentum operator. Since our projectors are diagonal with respect to the spin−orbit term $\sigma\cdot\mathbf{L}$, the implementation of this term is direct and compiler can optimize the code more efficiently. Note that the spin−orbit interaction is now coupled in the nonlocal interaction in a non-perturbative fashion and that the spin-components of an arbitrary wave function are mixed by this interaction term. This approach allows the inclusion of spin−orbit effects in an accurate manner with only a small increase in computational costs. Since a spinor wave function with two components is needed for each eigenstate, the number of plane-waves is effectively doubled (compared to a gamma point code, the cost is four times more components). Also the nonlocal potential now requires four times the amount of memory of a conventional code. While this increase is certainly not small, it is not prohibitive. The extra computational cost can be offset on parallel machines, since the nonlocal pseudopotential is easy to parallelize. The accuracy comes from the fact that the large majority of the spin−orbit effects comes from the core electrons. Assuming norm-conservation conditions are imposed, the electric field near each atom at or beyond the core cutoffs is nearly identical to one would find for an all-electron calculation since the core charge of the ion is preserved by the pseudopotential.

III. Applications

The Gaussian basis set calculations were performed with the development version of the NWDFT module of NWChem.[21] Molecules involving I, H, F, and Br were calculated using the 6-311G** basis set, and for those involving Au and Bi, large uncontracted basis sets[32] Au(26s20p19d16f) and Bi(26s23p19d14f) were used. Numerical integration was performed using the extremely fine integration grids available within NWChem.[25] All calculations were performed with spherical basis sets. In this paper, we have performed calculations with three different exchange-correlation functionals (LDA, PBE96, B3LYP). In each of the cases, the spin−orbit effects are discerned by comparing the spin-free case to that of the two-component spinor approach.

The plane wave calculations were done with the development version of the NWPW module of NWChem.[21] A cubic box of $20a_0$ was chosen with a cutoff energy of 101 Rydbergs for the wave function and 202 Rydbergs for the density for the PBE96 exchange-correlation functional calculations. Tests using this functional were also done using a smaller density grid (equal to that of the wave function) and showed insignificant differences for the reported properties of the molecules in the test suite confirming that the cutoff is adequate. However, changes in the vibrational frequencies of the gold dimer and gold hydride were noted. For comparison to the more accurate GGA(PBE96) results, calculations using the LDA or SVWN functional were completed using a cutoff of 101 Rydbergs for both the wave function and the density. The pseudopotential generation was done with the SVWN exchange-correlation functional. Since each test case is a closed shell molecular dimer, the initial wave function is taken to have multiplicity of one. The core radii, electronic configuration, maximum angular momentum, local pseudopotential used for the Kleinman-Bylander expansion, and the exact type of pseudopotential used for each molecule are given in Tables 4 and 5. Except for the H and F atoms, the core radii were generated based upon the default criteria of Hamann or Troullier−Martin for the corresponding pseudopotential.[29,30] This very stringent criteria was used in order to make the pseudopotentials as transferable as possible. It should be noted that these criteria will result in slightly different core radii for scalar relativistic and relativistic pseudopotentials. By default, the local pseudopotential used in the Kleinman−Bylander expansion was taken to be the pseudopotential for the maximum angular momentum. However, when ghost states were found a different angular momentum was chosen. The evidence for such a ghost state was taken to be the presence of a molecular bound state energy with a very low energy compared to the energy of the lone atom. For example, in Br the ghost state was 3 times lower in energy than the corresponding atomic orbital energy. In general, Hamann type pseudopotentials were used as a default and for all the relativistic two component pseudopotentials. Troullier−Martins type pseudopotentials were used only for cases where we had difficulty making the Hamann potentials work. However in most cases, there was no discernible difference in the quality between Hamann and Troullier−Martins potentials. In the radial Dirac or radial ZORA solver, the occupancies for the relativistic orbitals were determined by multiplying the total occupancy of the nonrelativistic orbital by the fraction of states for the relativistic orbital. For example, for a $5p^5$ state there are 6 states, the $5p_{1/2}$ state has 2 states while the $5p_{3/2}$ would have 4. Thus, the number of electrons in the $5p_{1/2}$ is $5 \times 2/6 = 5/3$, and the number of electrons in the $5p_{3/2}$ is $5 \times 4/6 = 10/3$. The yields a spherical potential for the relativistic case.

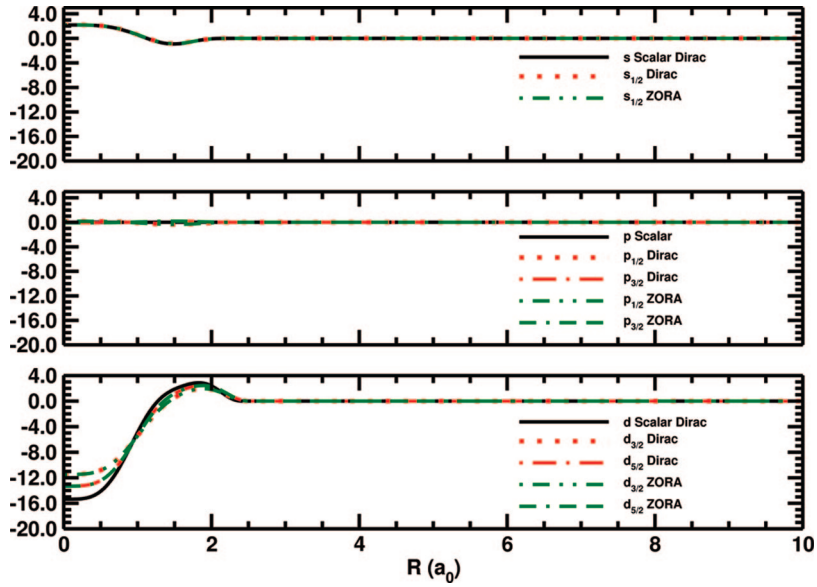

Figure 6. Radial components of the nonlocal spin-angular projectors (**L** = s, p, d) for bismuth using Scalar Dirac, Dirac, and ZORA.

Table 1. Bond Lengths (Å)

	I_2	IF	HI	Br_2	Bi_2	AuH	Au_2
experiment[34]	2.67	1.91	1.61	2.28	2.66	1.52	2.42
PW-PBE96-HGH-SO	2.67	1.97	1.61	2.28	2.57	1.54	2.53
PW-LDA-SR	2.67	1.87	1.63	2.29	2.62	1.60	2.47
PW-PBE96-SR	2.68	1.99	1.60	2.28	2.63	1.52	2.50
PW-PBE96-SO	2.61	1.90	1.62	2.27	2.57	1.59	2.61
GB-PBE96-ZORA-SR	2.71	1.94	1.63	2.32	2.65	1.55	2.54
GB-PBE96-ZORA-SO	2.73	1.95	1.63	2.33	2.68	1.55	2.52
GB-LDA-ZORA-SR	2.68	1.92	1.62	2.29	2.61	1.54	2.46
GB-LDA-ZORA-SO	2.70	1.92	1.63	2.29	2.64	1.54	2.45
GB-B3LYP-ZORA-SR	2.73	1.93	1.62	2.33	2.64	1.55	2.54
GB-B3LYP-ZORA-SO	2.75	1.93	1.62	2.33	2.69	1.55	2.53
GAMESS-UK-PBE96-GGA-SR[33]	2.70	1.91	1.61		2.61	1.53	2.46
GAMESS-UK-PBE96-GGA-SO[33]	2.72	1.92	1.62		2.64	1.53	2.45

Table 2. Vibrational Frequencies (cm^{-1})

	I_2	IF	HI	Br_2	Bi_2	AuH	Au_2
experiment[34]	215	610	2309	325	173	2305	191
PW-PBE96-HGH-SO	216	634	2263	327	199	2212	173
PW-LDA-SR	224	616	2249	331	187	3531	549
PW-PBE96-SR	217	610	2270	322	206	2250	185
PW-PBE96-SO	225	620	2315	323	201	2006	167
GB-PBE96-ZORA-SR	209	607	2247	308	192	2204	173
GB-PBE96-ZORA-SO	196	603	2228	305	177	2206	175
GB-LDA-ZORA-SR	221	639	2261	325	202	2267	193
GB-LDA-ZORA-SO	207	635	2239	321	168	2295	195
GB-B3LYP-ZORA-SR	209	626	2287	310	198	2186	169
GB-B3LYP-ZORA-SO	198	623	2268	307	166	2241	173

Table 3. Dissociation Energies (eV)

	I_2	IF	HI	Br_2	Bi_2	AuH	Au_2
experiment[34]	1.56	2.92	3.20	2.00	2.03	3.36	2.31
PW-LDA-SR	2.69	3.97	3.90	3.06	3.38	3.99	3.44
PW-PBE96-SR	2.13	2.95	3.40	2.59	4.20	3.28	2.40
PW-PBE96-SO	1.30	2.80	3.05	2.03	4.05	2.72	1.87
GB-PBE96-ZORA-SR	2.38	3.50	3.03	2.43	2.62	3.53	2.55
GB-PBE96-ZORA-SO	1.87	3.29	2.87	2.22	2.08	3.52	2.52
GB-LDA-ZORA-SR	2.92	4.30	3.76	3.10	3.51	3.64	3.06
GB-LDA-ZORA-SO	2.26	4.01	3.42	2.82	2.85	3.62	3.02
GB-B3LYP-ZORA-SR	2.52	3.05	3.19	2.11	2.45	3.48	3.48
GB-B3LYP-ZORA-SO	1.96	2.81	2.96	1.86	1.83	3.48	3.48

The Dirac solver was used for all calculations except for those noted below. To the best of the authors knowledge, this is first test of a norm conserving spin−orbit pseudopotential for most of these molecular dimers (except for a very recent paper[20] which calculated Au_2 and AuH). Hence for most of these molecules, the results can only be compared with the HGH spin−orbit pseudopotential [13]and Gaussian basis set ZORA DFT results. For Bi_2, I_2, and Au_2, tests were conducted at a lower cutoff ($32 \times 32 \times 32$ Fourier grid) to determine the optimal values for the local potential, maximum angular momentum, and pseudopotential type.

The results for the bond lengths are presented in Table 1 while vibrational frequencies are presented in Table 2. The dissociation energies are given in Table 3. For most of these molecules, the spin−orbit effect is small. This is expected since these molecules are closed shell. One will note that in some cases, the spin−orbit does not seem to improve things, though the correction is not significant and this disagreement might easily result from other factors. In general, one might expect that the spin−orbit interaction will drive the bond length to be slightly longer. The rationale for this type of effect is that the spin−orbit interaction splits the $2(2l + 1)$ degenerate atomic orbitals for a given l into two separate groups having total

Table 4. Planewave Pseudopotentials

atom	local	L_{max}	config	type
Br	d	d	$4s^2 4p^5$	TM
Bi	d	d	$6s^2 6p^2 6d^1$	Ham
I	d	d	$5s^2 5p^5$	Ham
Au	s	d	$5s^2 5p^6 5d^{10}$	TM
F	d	d	$2s^2 2p^5$	Ham
H	p	p	$1s^1$	Ham
Br	p	d	$4s^2 4p^5$	Ham
Bi	p	d	$6s^2 6p^3$	TM
I	p	d	$5s^2 5p^5$	Ham
Au	s	d	$5s^2 5p^6 5d^{10}$	Ham

Table 5. Planewave Radial Cutoffs for Pseudopotentials (a_0)

	Br	Bi	I	H	Au	F
s	1.405	1.114	1.0130	0.800	0.844	0.700
p	1.657	1.466	1.2062	0.800	0.951	0.700
d	1.657	1.958	1.4733		1.215	0.700
$s_{1/2}$	0.843	1.866	1.013		0.506	
$p_{1/2}$	0.979	2.211	1.171		0.535	
$p_{3/2}$	0.999	2.542	1.224		0.585	
$d_{3/2}$	1.706	2.542	1.466		0.714	
$d_{5/2}$	1.715	2.542	1.481		0.740	

angular momenta of $j = l + {}^1/_2$ and $j = l - {}^1/_2$. The $j = l - {}^1/_2$ component is $2l$ degenerate and is slightly pushed in toward the nucleus with respect to the nonrelativistic or scalar relativistic reference, while the $j = l + {}^1/_2$ component is $2l + 2$ degenerate and pushed away from the nucleus. This effect can be seen in Figure 2 for the Bi pseudowave functions. The net result is that one may expect the bonding region to move away from the nuclei and create a slightly longer bond when spin−orbit effects are included. This type of effect is seen for the I_2 and Bi_2 dimers in the Gaussian ZORA basis set calculations; however, this effect is not readily observed for the other dimers. This type of effect was not observed in the planewave basis set calculations. The most likely reason for this is that the differences associated with the subtle differences in parameters for generating the scalar relativistic and spin−orbit relativistic pseudopotentials are large enough to wash out this effect. Similar results have been observed in a previous plane-wave study by Oda and coworkers[19] using ultrasoft fully relativistic pseudopotentials for solid-state calculations. For Pb and Pt an increase in the equilibrium lattice constant is observed while for Au a decrease is noted. There are many competing effects that do not directly derive from the spin−orbit potential which might have influences on the bond lengths such as the image interaction or box effects. For most cases, there is good agreement between experiment and theory. The Gaussian ZORA appears to yield much smaller spin−orbit effects than the relativistic Dirac planewave pseudopotential. Comparing these results to that of the all-electron DFT ZORA implementation in GAMESS-UK,[33] one sees very close agreement. The differences are less than five percent in all cases. Also one sees close agreement with the results for the planewave method with HGH pseudopotentials (note these results were generated by NWChem and, while very close to those published originally in the HGH paper,[13] are not identical).

For dissociation energies, the same trend is observed as with the bond lengths. As one would expect, LDA tends to give better geometries while GGA yields better dissociation energies. The inclusion of spin−orbit seems to improve the dissociation energy somewhat. Once again the Gaussian ZORA agree well with the results from Faas et al.[33] As for the harmonic frequencies, most of these follow a trend similar to what is observed in other quantities. In agreement with physical intuition, a shorter bond length leads to a higher harmonic frequency and vice versa. One notable exception was found in the planewave calculations for the dimers IF, AuH, and Au_2 where initial tests yielded very large frequencies even when the dissociation energies and bond lengths were nearly equal the experimental values. The problem was found to be that F and Au both have very small compact pseudowave functions using the default parameters of Hamann or Troullier−Martin. It was found that the frequencies for Au_2 and AuH could be made to approach the experimental values when larger cutoff radii were used to define the Au pseudopotential. Unfortunately, increasing the cutoff radii resulted in large errors in the dissociation energy. The lack of transferability of the Au pseudopotential is likely the result of the core states of Au being highly polarizable, and a very large cutoff is needed to resolve the compact core functions. To address this effect, the 5s, 5p, and 5d orbitals were included in the valence space. Even though these pseudopotentials produced better results than without the 5s and 5p state. Table 1 still shows a need for improvement. For Gaussian basis sets, a very diffuse set is needed to properly represent the metallic bonding aspects of this molecule. Nevertheless, the results are reasonable. Past calculations such a that of Naveh et al. found bond lengths of 2.55 for this dimer.[20] Scalar ZORA calculation by van Lenthe et al.[8] found 2.458 and 2.517 Å for LDA and GGA, respectively. The Gaussian ZORA DFT results of 2.45 and 2.52 Å are very close to the previously reported results. The planewave result of 2.50 Å is nearly the same as the scalar ZORA; however, the inclusion of spin−orbit effects actually makes the agreement with the experimental bond length, 2.42 Å, slightly worse. Note that an experimental value of 2.47 Å has also been reported. For AuH, the calculated values of 1.539 for scalar ZORA, 1.55 for the real-space method, 1.55 for the present Gaussian ZORA DFT, and 1.52 for the present planewave method all compare somewhat well with the experimental value of 1.52 Å. Once again for the gold pseudopotential, the planewave results are slightly elongated with the addition of the spin−orbit coupling for bond lengths and the addition of spin−orbit in the planewave case actually leads to slightly less accurate predictions. This addition has no visible effect in the Gaussian ZORA DFT approach.

IV. Conclusions

Relativistic two-component methods have been implemented in the NWChem program within the molecular Gaussian DFT and pseudopotential planewave DFT modules. These methods have been shown to produce reliable results for the small closed-shell molecules we have considered in this paper. These two methods are also complementary. The all-electron Gaussian ZORA DFT method allows one to calculate relativistic properties of molecules with albeit expensive costs compared with RECP DFT while the planewave method

allows a more economical approach. Also the planewave method will allow calculations of surfaces, solids, and solutions in a completely ab initio manner, while the Gaussian basis set will allow the calculation of properties associated with core electrons. These two implementations will be available within the quantum chemistry program NWChem. The planewave method builds on previous implementations[13−19] of similar pseudopotentials and opens the possibility of performing spin−orbit calculations on thousands of processors. Likewise, the Gaussian basis set all-electron ZORA implementation provides similar capabilities. Future work includes the application of these methods to open shell heavy atom compounds, in particular, actinide and lanthanide compounds. While these methods are certainly cheap compared with more traditional approaches, they provide chemists with the ability to include a realistic description of relativistic effects such as spin−orbit splitting, molecular orbital hybridization, and core effects.

Acknowledgment. This research was supported by the BES Heavy Element Chemistry Program of the U.S. Department of Energy, Office of Science (No. DE-AC06-76RLO 1830). E.J.B. would like to acknowledge the DOE BES Geosciences Program for helping support the development of the AIMD and analysis programs. The Pacific Northwest National Laboratory is operated by the Battelle Memorial Institute. Some of the calculations were performed on the MPP2 computing system at the Molecular Science Computing Facility in the William R. Wiley Environmental Molecular Sciences Laboratory (EMSL) at PNNL. EMSL operations are supported by the DOE's Office of Biological and Environmental Research. We also wish to thank the Department of Energy for a grant of computer time at the National Energy Research Scientific Computing Center (Berkeley, CA).

References

(1) Barysz, M. *J. Chem. Phys.* **2000**, *113*, 4003.

(2) Dyall, K. G. *J. Chem. Phys.* **1994**, *100*, 2118.

(3) Douglas, M.; Kroll, N. M. *Ann. Phys. (N.Y.)* **1974**, *82*, 89.

(4) Wolf, A.; Reiher, M.; Hess, B. A. *J. Chem. Phys.* **2002**, *117*, 9215.

(5) Hess, B. A. *Phys. Rev. A* **1985**, *32*, 756. **1986**, *33*, 3742. .

(6) Chang, Ch.; Pelissier, M.; Durand, Ph. *Phys. Scr.* **1986**, *34*, 394.

(7) van Lenthe, E.; Baerends, E. J.; Snijders, J. G.; Zhang, J. *J. Chem. Phys.* **1993**, *99*, 4597.

(8) Van Lenthe, E.; Baerends, E. J.; Snijders, J. G. *J. Chem. Phys.* **1994**, *101*, 9783.

(9) van Lenthe, E.; Snijders, J. G.; Baerends, E. J. *J. Chem. Phys.* **1996**, *105*, 6505.

(10) Pacios, I. F.; Christiansen, P. A. *J. Chem. Phys.* **1985**, *82*, 2664.

(11) Hay, P. J.; Wadt, W. R. *J. Chem. Phys.* **1985**, *82*, 299.

(12) Hay, P. J.; Wadt, W. R. *J. Chem. Phys.* **1985**, *82*, 270.

(13) Hartwigsen, C.; Goedecker, S.; Hutter, J. *Phys. Rev. B* **1998**, *58*, 3641.

(14) Dal Corso, A.; Conte, A. M. *Phys. Rev. B* **2005**, *71*, 115106.

(15) Dal Corso, A. *Phys. Rev. B* **2007**, *76*, 054308.

(16) Hemstreet, L. A.; Fong, C. Y.; Nelson, J. S. *Phys. Rev. B* **1993**, *47*, 4238.

(17) Theurich, G.; Spaldin, N. *Phys. Rev. B* **2001**, *64*, 073106.

(18) Theurich, G.; Spaldin, N. *Phys. Rev. B* **2002**, *66*, 115208.

(19) Oda, T.; Hosokawa, A. *Phys. Rev. B* **2005**, *72*, 224428.

(20) Naveh, D.; Kronik, L.; Tiago, M. L.; Chelikowsky, J. R. *Phys. Rev. B* **2007**, *76*, 153407.

(21) Bylaska, E. J.; de Jong, W. A.; Govind, N.; Kowalski, K.; Straatsma, T. P.; Valiev, M.; Wang, D.; Apra, E.; Windus, T. L.; Hammond, J.; Nichols, P.; Hirata, S.; Hackler, M. T.; Zhao, Y.; Fan, P.-D.; Harrison, R. J.; Dupuis, M.; Smith, D. M. A.; Nieplocha, J.; Tipparaju, V.; Krishnan, M.; Wu, Q.; Van Voorhis, T.; Auer, A. A.; Nooijen, M.; Brown, E.; Cisneros, G.; Fann, G. I.; Fruchtl, H.; Garza, J.; Hirao, K.; Kendall, R.; Nichols, J. A.; Tsemekhman, K.; Wolinski, K.; Anchell, J.; Bernholdt, D.; Borowski, P.; Clark, T.; Clerc, D.; Dachsel, H.; Deegan, M.; Dyall, K.; Elwood, D.; Glendening, E.; Gutowski, M.; Hess, A.; Jaffe, J.; Johnson, B.; Ju, J.; Kobayashi, R.; Kutteh, R.; Lin, Z.; Littlefield, R.; Long, X.; Meng, B.; Nakajima, T.; Niu, S.; Pollack, L.; Rosing, M.; Sandrone, G.; Stave, M.; Taylor, H.; Thomas, G.; van Lenthe, J.; Wong, A.; Zhang, Z. *NWChem, A Computational Chemistry Package for Parallel Computers*; version 5.1, Pacific Northwest National Laboratory: Richland, WA, 2007; 99352−0999.

(22) van Wüllen, C. *J. Chem. Phys.* **1998**, *109*, 392.

(23) van Lenthe, E.; Ehlers, A.; Baerends, E.-J. *J. Chem. Phys.* **1999**, *110*, 8943.

(24) Filatov, M.; Cremer, D. *J. Chem. Phys.* **2005**, *122*, 44104.

(25) (a) Murray, C. W.; Handy, N. C.; Laming, G. L. *Mol. Phys.* **1993**, *78*, 997. (b) Mura, M. E.; Knowles, P. J. *J. Chem. Phys.* **1996**, *104*, 9848. (c) Treutler, O.; Alrhichs, R. *J. Chem. Phys.* **1995**, *102*, 346. (d) Lebedev, V. I.; Laikov, D. N. *Doklady Mathematics* **1999**, *366*, 741. (e) Becke, A. D. *J. Chem. Phys.* **1988**, *88*, 1053. (f) Stratmann, R. E.; Scuseria, G.; Frisch, M. J. *Chem. Phys. Lett.* **1996**, *257*, 213. (g) Gill, P. M. W.; Johnson, B. G.; Pople, J. A. *Chem. Phys. Lett.* **1993**, *209*, 506–512.

(26) Van Lenthe, J. H.; Faas, S.; Snijders, J. G. *Chem. Phys. Lett.* **2000**, *328*, 107.

(27) Van Lenthe, J. H.; van Lingren, J. N. J. *Int. J. Quantum Chem.* **2006**, *106*, 2525.

(28) Sakurai, J. J. *Advanced Quantum Mechanics*, 10th ed.; Addison Wesley Publishing Co.: Reading, MA, 1967.

(29) Hamann, D. R. *Phys. Rev. B* **1989**, *40*, 2980.

(30) Troullier, N.; Martins, J. L. *Phys. Rev. B* **1991**, *43*, 1993.

(31) Kleinman, L.; Bylander, D. M. *Phys. Rev. Lett.* **1982**, *48*, 1425.

(32) Tatewaki, H.; Koga, T. *Chem. Phys. Lett.* **2000**, *328*, 473.

(33) Faas, S.; Van Lenthe, J. H.; Hennum, A. C.; Snijders, J. G. *J. Chem. Phys.* **2000**, *113*, 4052.

(34) Huber, K. P.; Herzberg, G. (data prepared by Gallagher, J. W.; Johnson, R. D., III.) Constants of Diatomic Molecules. In NIST Chemistry WebBook, NIST Standard Reference Database Number 69; Linstrom, P. J., Mallard, W. G., Eds.; National Institute of Standards and Technology: Gaithersburg, MD, June 2005; http://webbook.nist.gov (accessed June 1, 2008).

CT8002892